Functional phenomics and genetics of the root economics space in winter wheat using high-throughput phenotyping of respiration and architecture

Haichao Guo[1], Habtamu Ayalew[1], Anand Seethepalli[1], Kundan Dhakal[1], Marcus Griffiths[1], Xue-Feng Ma[1], Larry M. York[1]

[1]Noble Research Institute, LLC, 2510 Sam Noble Parkway, Ardmore, OK 73401

Author for correspondence:

Larry M. York

Tel: +1 5802246720

Email: lmyork@noble.org

Summary

- The root economics space is a useful framework for plant ecology, but rarely considered for crop ecophysiology. In order to understand root trait integration in winter wheat, we combined functional phenomics with trait economic theory utilizing genetic variation, high-throughput phenotyping, and multivariate analyses.
- We phenotyped a diversity panel of 276 genotypes for root respiration and architectural traits using a novel high-throughput method for CO_2 flux and the open-source software RhizoVision Explorer for analyzing scanned images.
- We uncovered substantial variation for specific root respiration (SRR) and specific root length (SRL), which were primary indicators of root metabolic and construction costs. Multiple linear regression estimated that lateral root tips had the greatest SRR, and the residuals of this model were used as a new trait. SRR was negatively correlated with plant mass. Network analysis using a Gaussian graphical model identified root weight, SRL, diameter, and SRR as hub traits. Univariate and multivariate genetic analyses identified genetic regions associated with aspects of the root economics space, with underlying gene candidates.
- Combining functional phenomics and root economics is a promising approach to understand crop ecophysiology. We identified root traits and genomic regions that could be harnessed to breed more efficient crops for sustainable agroecosystems.

Key words: GWAS, multi-trait, root architecture, root respiration, winter wheat

Introduction

Functional phenomics is an emerging transdisciplinary field that integrates physiology, high-throughput phenotyping, and computational biology in order to fill knowledge gaps about plant functioning (York, 2019). High-throughput phenotyping allows for large-scale data collection on plant form and function, and is often used for genetics within a species. Phenomics focuses on understanding variation in plant phenotypes, but often lacks analysis of the relation of phenotypes to function, even if quantitative genetics are employed. Therefore, functional phenomics is needed using statistical associations within high-dimensional phenomics data to infer how traits influence one another and physiological processes important for crop growth. Especially, root phenomics data and conceptual frameworks are lacking to understand their interactions and integration as described in York *et al.* (2013). The trait economics spectrum is a conceptual framework from ecology that could help explore trait integration in crops. In this context, economics refers to the balance among traits for resource acquisition and utilization, with an explicit treatment of the tradeoffs between pairs of traits (Reich, 2014). For example, in a controlled study of 74 plant species, a root economics spectrum was found in which root respiration correlated to percent nitrogen, root length per unit mass, and the decomposition rate of dried roots in soil (Roumet *et al.*, 2016). Recently, a root economics space was proposed formed by one axis representing whether to cooperate with fungal partners and a second representing the 'fast' or 'slow' strategies (Bergmann *et al.*, 2020). Interestingly, the first axis was partially driven by specific root length relating to construction cost, and the second axis by root nitrogen content, a proxy of specific root respiration and metabolic cost. Therefore, the root economics space is a useful framework for understanding carbon use efficiency in crop roots.

Roots are the interface between plants and soil, with a key function to extract nutrients and water that are required for plant productivity (Smith & De Smet, 2012; Meister *et al.*, 2014). However, there is a complex relationship between investing in the root system and plant productivity because roots have a cost. The fraction of newly fixed carbon from photosynthesis allocated to roots can exceed 50%, and this proportion to roots significantly increases under edaphic stress (Lambers *et al.*, 1996; Rachmilevitch *et al.*, 2015). Root system carbon costs can be classified as construction costs, including the structure of the roots and growth respiration,

and maintenance costs, primarily respiration and exudation (Mooney, 1972; Sun *et al.*, 2020). For example, in wheat seedlings, 30% of net photosynthesis was measured as root construction and maintenance costs, such as respiration (Sawada, 1970). Therefore, optimizing construction and metabolism of the root system would have a significant impact on plant carbon use efficiency.

Specific root length is a measure of carbon expenditure to construct root length, often in units of m g^{-1}. Specific root respiration standardizes respiration based on root length or mass, typically with units of nmol CO_2 s^{-1} cm^{-1} or mg^{-1}, respectively. Specific root length was found to have variation among a set of barley and wheat lines but the genetic contribution was not considered explicitly (Løes & Gahoonia, 2004), and was used for QTL analysis in common bean (Ochoa *et al.*, 2006). Across the plant kingdom, as much as 52% of photosynthates may be respired by plant roots during the same day, depending on species and environmental conditions (Lambers *et al.*, 1996). Plants respire photosynthetic substrates to produce carbon skeletons, usable energy, and chemical reduction needed for development (Amthor, 2000), which results in the consumption of oxygen and the release of carbon dioxide. A multicomponent framework has been suggested to divide respiration into (1) growth fraction, biosynthesis of new structural biomass and exudates, (2) maintenance fraction, translocation of photosynthate from sources to sinks, and cellular ion-gradient maintenance, (3) ion-uptake fraction, including uptake of ions, assimilation of N and S, and protein turnover (McCree, 1970; Thornley, 1970; Johnson, 1983; Poorter *et al.*, 1991; Amthor, 2000). As up to 60% of assimilated carbon is lost through respiration, strategies to minimize unnecessary respiratory activity could lead to substantial gains in crop productivity by enhancing plant carbon use efficiency (Amthor *et al.*, 2019; Weber & Bar-Even, 2019; Roell & Zurbriggen, 2020).

Variation in root respiration rates among crop species is due to the differences in root tissue density, anatomy, activity, chemistry, and structure (Ben-Noah & Friedman, 2018). Studies have shown that reducing root respiration through anatomical changes such as root cortical senescence of barley (*Hordeum vulgare* L.) and wheat (*Triticum aestivum* L.) (Schneider *et al.*, 2017) or reduction in root secondary growth of common bean (*Phaseolus vulgaris* L.) (Strock *et al.*, 2018) permit greater plant growth by improving phosphorus capture from low-phosphorus soils. Strategies have been proposed or used to reduce root respiratory carbon cost for improving plant performance, including making ion transport more efficient

(Amthor *et al.*, 2019), manipulation of genes or enzymes involved in carbon metabolism in plant roots (Dorion *et al.*, 2017; Florez-Sarasa *et al.*, 2020), and using arbuscular mycorrhizal symbiosis to reduce root respiratory rate as well as increasing photosynthesis (Romero-Munar *et al.*, 2017). Root respiration that is not accounted for necessary plant functions might be referred to as luxury respiration.

Understanding the genetic bases of specific root length and respiration, among other traits, and their relationship to plant performance is of key importance for breeding more productive and resilient crop varieties to adapt to climate change. However, these traits have rarely been considered as a unit of phenotype for breeding or genetic mapping. Genome-wide association studies (GWAS) for respiratory traits will typically require many hundreds of plant variants, and measurement of respiratory traits at the same time of day and developmental stage (Scafaro *et al.*, 2017). Infrared gas analyzers for portable leaf photosynthesis or O_2-electrodes techniques are commonly used to measure rates of root respiration (Poorter *et al.*, 1991; Strock *et al.*, 2018), but most of those protocols are low-throughput with costly instruments that have less flexibility for outputting convenient data formats. Addressing the need for rapid, cost-effective, large-scale root respiratory screening will require the development of both high-throughput root respiration measurement and data analysis capabilities, the combination of which will greatly strengthen functional phenomics by increasing statistical power and enabling genetic mapping (York, 2019).

Wheat, a member of the grass family, is an important cereal grown globally. Winter wheat in the Southern Great Plains of the United States is often grown as a dual-purpose crop for forage and grain production (Maulana *et al.*, 2019). Yield, protein content (Rajaram, 2001), disease resistance (Ellis *et al.*, 2014), and heat resistance (Maulana *et al.*, 2018) are major targets for modern wheat breeding and genetic improvement. Significant marker-trait associations for aboveground traits, such as yield and its components (Sukumaran *et al.*, 2018) and nitrogen use efficiency (Cormier *et al.*, 2016; Hawkesford & Griffiths, 2019), have been reported across the wheat genome. Indeed, considerable quantitative trait loci (QTL) associated with wheat root traits have been identified on nearly all chromosomes in variable environments (Hamada *et al.*, 2012; Bai *et al.*, 2013; Atkinson *et al.*, 2015; Maccaferri *et al.*, 2016; Xie *et al.*, 2017; Beyer *et al.*, 2019; Soriano & Alvaro, 2019). However, the genetic and functional basis of root traits still lag behind aboveground traits, and genetic variation of root construction and metabolic traits

remains less explored. Accordingly, this study was conducted to (1) develop a high-throughput phenotyping platform that integrates a hydroponics growth system, infrared gas analyzers, custom gas chambers, a bead bath, flatbed scanners, analytical scales, and an R script for measuring specific root respiration, specific root length, and other root traits, (2) validate the platform using winter wheat to uncover heritable variation of root respiration and architectural traits, (3) emply functional phenomics to identify relations among traits and tissue-type dependencies, and (4) identify associated QTL/genes that drive root respiration and other root traits by performing GWAS.

Materials and Methods

Plant materials

The plant materials were selected from the hard winter wheat association mapping panel (HWWAMP) by the Triticeae Coordinated Agricultural Project (T-CAP). Two hundred seventy-six hard winter wheat cultivars and breeding lines were selected from the panel, which covers a broad range of selection and breeding history in the Great Plains of the USA.

Experimental design

The 276 wheat lines were grown as two replicates in a single growth chamber with 552 plants, with the entire procedure repeated twice, for a total of four replicates and 1104 plants evaluated in this study. Each replicate was treated as a block for an overall experiment with a randomized complete block design. The two transplanting dates of seedlings into the growth hydroponics boxes were June 19 and October 4 in 2019. The details of the germination, growth, and sampling are given below.

Growth conditions

Seeds were surface-sterilized in 0.5% NaOCl for 10 min and rinsed three times using deionized (DI) water, then pre-germinated in petri dishes with filter paper placed in darkness at 25 °C for 3 d. Uniformly germinated seedlings were selected (Figure 1a), wrapped around the root-shoot junction with L800-D Identi-Plugs foam (Jaece Industries, NY, USA), plugged in a 15 mL conical centrifuge tube (VWR, Falcon®, catalog number: 21008-918) with the bottoms cut away from the “6 ml” mark, and transplanted to a hole cut into the lid of the growth system as described below (Figure 1b). A unique barcode label was affixed to each tube for sample identification. The hydroponics growth system consisted of a polypropylene divider box (inside dimensions: length of 38.10 cm, width of 22.86 cm, and height of 20.32 cm with a volume of 17.7 L) and a custom

lid made from a PVC panel cut to fit in the top of a box (4.5 mm thick, by 250 mm wide, by 392 mm long with the corners cut off to accommodate the box's rounded corners). Forty-eight holes with 18 mm diameter were drilled into the lid with a hole saw with equal spacing among holes. Twelve growth boxes were placed in a Conviron E-15 growth chamber (Conviron, Winnipeg, Canada) with a day:night cycle of 16:8 h, 25:20 °C, at a flux density at canopy level of ~400 µmol m^{-2} s^{-1}. Each box was filled to the bottom of the lid with a nutrient solution containing (µM) 125 KH_2PO_4, 1125 KNO_3, 500 $CaCl_2$, 250 $MgSO_4$, 11.5 H_3BO_3, 1.75 $ZnSO_4 \cdot 7H_2O$, 2.25 $MnCl_2 \cdot 4H_2O$, 0.08 $CuSO_4 \cdot 5H_2O$, 0.03 $(NH_4)_6Mo_7O_{24} \cdot 4H_2O$, and 19.25 Fe(III)-EDTA ($C_{10}H_{12}N_2NaFeO_8$). The nutrient solution was continuously aerated with an air pump attached to airstones submerged in each growth box, and the solution pH was maintained between 5.9 and 6.1 by additions of KOH or HCl throughout the experiment.

High-throughput root respiration measurements

Ten days after transplanting (Figure 1c), plants were removed from the nutrient solution. Roots were immediately excised from shoots, blotted using tissue paper to remove excess water, placed in a 19 ml custom chamber, and then the chamber connected to an LI-850 CO_2/H_2O Analyzer (LI-COR Inc., NE, USA) (Figure 1d). The custom chamber was made from a 12.70 mm internal diameter clear polyvinyl chloride (PVC) pipe nipple (United States Plastic Corp., OH, USA) that was 152.4 mm in length with threaded ends. Holes were drilled into ½ inch FNPT nylon threaded caps (United States Plastic Corp., OH, USA) in order to accommodate insertion of quick-connect bulkhead male or female fittings (LI-COR Inc., NE, USA) with rubber grommets to create a seal. A Balston filter (LI-COR Inc., NE, USA) was inserted between the chamber and the analyzer to filter air. The chamber was buried in a Lab Armor bead bath (Model No 74300-714) filled with Lab Amor metallic beads with the temperature set at 28 °C. Beads were preferred to water in order to prevent contamination of the system with water. The chamber CO_2 concentration was continuously recorded using LI-850 Windows software v 1.0.2 for 90 seconds at a rate of one reading per second. A USB barcode scanner (Taotronics, Fremont, CA) was connected to each laptop to acquire and save the datafile with the appropriate sample name encoded by the barcode affixed to the cut tube described above. Three infrared gas analyzers were used to allow simultaneous measurements in parallel to increase throughput.

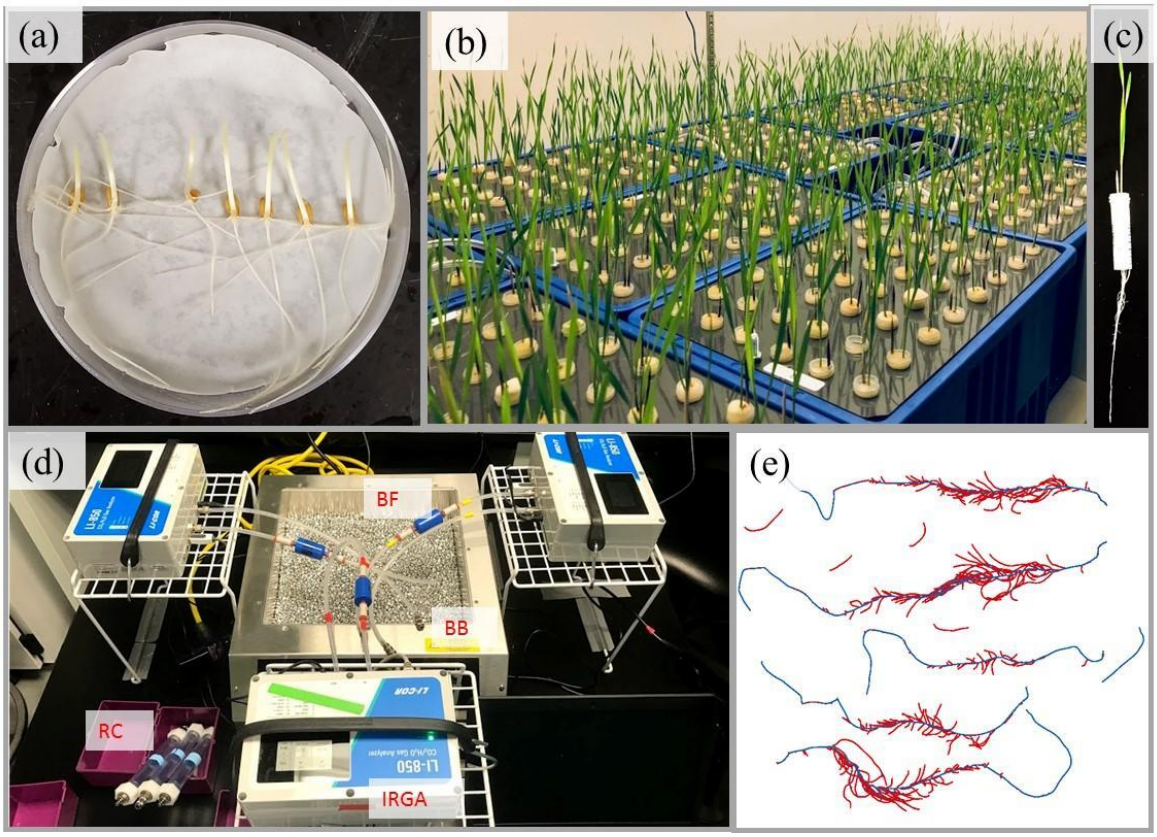

Figure 1 Platform for phenotyping root respiration and other root traits of wheat seedlings. (a) Wheat seeds were surface sterilized and pre-germinated in plate, (b) Seedlings were grown in aerated hydroponics for 10 days, (c) Shoot and roots of seedling 10 days after transplanting, (d) Root respiration was measured in bead bath using Li-850, (e) Distinguish axial roots (blue) from lateral roots (red) of the scanned image using RhizoVision Explorer. IRGA: Infrared gas analyzer, RC: Root chamber, BB: Bead bath, BF: Balston filter.

In order to calculate the total respiration rate of a root sample from the individual text files containing the time series molar fraction of CO_2, an R (R Core Team, 2018) script was developed in order to load each text file in a directory, do a series of computations, and output the total respiration rate. Total respiration rate (CO_2 flux) was calculated using Equation 1.

$$F = \frac{PV}{RT}\frac{dC}{dt} \quad (1)$$

Where F is the CO_2 flux in nmol s^{-1}, P is the pressure in the chamber in kPa, V is the corrected chamber volume in milliliters, R is the ideal gas law constant in L kPa K^{-1} mol^{-1}, T is air temperature in K, and dC/dt is the change in CO_2 concentration on a molar basis with time (µmol mol^{-1} s^{-1}). Chamber volume (V) was determined by subtracting the total root volume estimated using RhizoVision Explorer from the chamber volume. For root respiration analysis, the dead band

(length of initial time to ignore) was set at 20 s. The slope of a linear regression fit to water-corrected CO_2 concentration provided by the LI-850 analyzer over the corresponding observation time (20-90 s) using the *lm* function in R (R Core Team, 2018) is dC/dt. The protocol for the root respiration measurements and the R script for calculating total flux from a directory of text files are available at https://doi.org/10.5281/zenodo.4247873 (Guo *et al.*, 2020a).

After the root respiration measurements, roots from each plant were spread in a 5 mm layer of water in transparent acrylic trays and imaged with a flatbed scanner equipped with a transparency unit (Epson Expression 12000XL, Epson America) at a resolution of 600 dpi. Images were analyzed using RhizoVision Explorer version 2.0.2 (Seethepalli & York, 2020) with algorithms described by Seethepalli *et al.* (2020) with the options for image thresholding level, filter noisy components, threshold for root pruning being set at 205 pixel intensity, 0.2 mm^2, and 1 pixel, respectively. A root diameter threshold of 0.30 mm was used to distinguish axial roots from lateral roots (Figure 1e).

Root traits extracted by the RhizoVision Explorer used in this study were number of root tips (Tip), number of branching points (BP), branching frequency (BF), total root length (TRL), axial root length (ARL), lateral root length (LRL), average diameter (AvgD), total root volume (TRV), axial root volume (ARV), lateral root volume (LRV), total root surface area (TSA), axial root surface area (ASA), and lateral root surface area (LSA). Branching frequency is determined by the software by dividing the number of branching points by total root length. Roots following scanning and shoots were dried at 60 °C for 3 days prior to dry weight determination. The oven-dried root mass and root length quantified using RhizoVision Explorer were used to calculate the specific root respiration (SRR) per unit of root dry mass (SRR_M; nmol g^{-1} s^{-1}) and the specific root respiration per unit of root length (SRR_L; nmol m^{-1} s^{-1}), respectively.

Root mass fraction (RMF) was calculated as root dry weight proportion of total plant dry weight. Specific root length (SRL) was calculated by dividing root length by the corresponding root dry weight. Lateral-to-axial root length ratio was calculated by dividing lateral root length by corresponding axial root length based on the diameter threshold provided during image analysis, and lateral-to-axial root volume ratio was calculated by dividing lateral root volume by corresponding axial root volume. Branching density (BD) was calculated by dividing root tips by axial root length. Root tissue density (RTD) was calculated by dividing root dry weight by root volume, which brought the total number of traits reported to 25 in this study.

Broad-sense heritability (H^2) of each trait was calculated based on Falconer and Mackay (1996) as:

$$H^2 = \frac{\sigma_g^2}{\sigma_g^2 + \frac{\sigma_e^2}{r}}$$

The variables σ_g^2, σ_e^2, and $r$represent the variance of the genotype effect, variance of the local environment effect, and the number of replicates (blocks), respectively. The variances were obtained by fitting to a mixed model including genotype as a random effect and block as a fixed effect using the lme4 package (Bates *et al.*, 2014).

Principal component (PC) analysis and visualization of outputs were performed on the trait means of the 25 traits using the base function "prcomp" and the R package "factoextra" (Kassambara & Mundt, 2017). The first ten principal component scores were extracted for clustering and PC-based GWAS analysis (PC-GWAS).

Network analysis

Due to highly correlated variables and singularities, root volume, surface area related traits, and lateral-to-axial root length ratio were dropped for network analysis. To assess the relationships among all the remaining 17 traits, we estimated pairwise Pearson's correlation coefficients (r) of the traits and constructed a Gaussian graphical model for network analysis. Network analysis with a Gaussian graphical model is more likely to capture causality and precursor/product relationships in trait networks relative to standard correlation analyses (Krumsiek *et al.*, 2011; Carlson *et al.*, 2019). The network analysis and the visualization of trait relationships were carried out with the R package 'qgraph' (Epskamp *et al.*, 2012). Outdegree is the number of connections that a trait node has to other trait nodes. Betweenness centrality quantifies the number of times a trait node acts as a bridge along the shortest path between two other trait nodes.

Multiple linear regression analysis

Multiple linear regression analysis was employed to determine how total respiration can be partitioned into the contributions from root tissue types. The total axial root volume, lateral root axis volume (minus the tip volume), and lateral root tip volume were considered as the dependent variables while the total root respiration was the independent variable. The number of lateral root tips was estimated by subtracting 4 from the number of root tips supplied by RhizoVision Explorer, assuming that the typical wheat seedling had 4 seminal roots. This

number of lateral roots was multiplied by 0.01 mm^3 in order to assign a small volume to the lateral root tips, which were assumed to be more active based on previous research. Lateral root axis volume was determined by subtracting lateral root tip volume from the total lateral root volume. Based on visual evaluation of feature images in RhizoVision Explorer, total lateral root volume and total axial root volume were assumed as the volumes of the diameter ranges ≤ 0.3 mm or > 0.3 mm, respectively. The "stepAIC" function as implemented in R package "MASS" (Ripley *et al.*, 2013) was used for the stepwise regression and revealed this full model as being the most parsimonious, so residuals of this model were used as an additional trait (SRR_R) for subsequent analysis. SRR_R is the respiration that is not accounted for after considering root system architecture and root tissue dependency.

SNP Genotyping

High-density single-nucleotide polymorphism (SNP) markers from the wheat 90K SNP genotyping array were obtained from Genotype Experiment "TCAP90K_HWWAMP" of The Triticeae Toolbox database (https://triticeaetoolbox.org/wheat/). Data constituting 21,555 SNPs were filtered to exclude markers with missing data greater than 50% and minor allele frequency less than 5%, resulting in 16,058 makers that were used in the association analysis. The map positions for the SNP markers used in this study were based on the consensus map developed using a combination of eight mapping populations (Wang *et al.*, 2014).

Genome-Wide Association Analysis

Three genome-wide association analysis approaches were employed to identify genomic regions associated with various root traits. The linear mixed model (LMM) in GEMMA (Zhou & Stephens, 2012; Zhou & Stephens, 2014) was used to test for association between SNPs and traits. The population relatedness matrix was estimated using the centered relatedness algorithm within GEMMA, and was chosen as a covariate in the model. A Wald test was performed to determine *p*-values.

Single-trait (Univariate) association testing was run for each of the 25 traits using mean phenotypic values and PC-GWAS was conducted using each of the first 10 PCs. Multi-trait (Multivariate) GWAS was carried out to increase the power of the association tests and to detect polymorphisms with potentially pleiotropic effects of trait-associated loci using the multivariate linear mixed effect modeling capabilities of GEMMA. The 25 traits were grouped into six multi-trait combinations based on their genetic correlations, or their structural and functional

relationships (McCormack *et al.*, 2017; Ben-Noah & Friedman, 2018). Root dry weight and shoot dry weight were combined to form a biomass-related multi-trait set (biomass). Total root respiration, root dry weight, root mass fraction, number of root tips, axial root length, and branching density were combined to form a root-respiration-related multi-trait set (root respiration) because these traits had functional relationships based on network analysis and provide a broader picture of root respiration. Axial root length, lateral root length, axial root volume, lateral root volume, axial root surface area, and lateral root surface area were combined to form a root-morphology-related multi-trait set (morphology). Branching point, branching frequency, and branching density were combined to form a root-topology-related multi-trait set (topology). Specific root length, root tissue density, and average root diameter were combined to form a root-construction-related multi-trait set (construction). Root mass fraction, lateral-to-axial root length ratio, and lateral-to-axial root volume ratio were combined to form an allocation-related multi-trait set (allocation). Multi-trait association was conducted with GEMMA using the multivariate version of the same model used for single-trait associations.

Outputs from GEMMA were used to generate Manhattan and Quantile–quantile (QQ) plots using the R package "qqman" (Turner, 2014). As mentioned in many wheat studies (Maulana *et al.*, 2018; Beyer *et al.*, 2019), determining a significance cutoff threshold is one of the biggest challenges for GWAS. Significant QTL were initially tested based on a false discovery rate of 0.05 following a stepwise procedure, which is very stringent (Müller *et al.*, 2011). So, an unadjusted significance level of $-\log_{10} P \geq 3.5$ was used for detecting SNPs that are significantly associated with the traits.

Identification of candidate genes

The sequences of significant markers associated with phenotypic traits were downloaded from the The Triticeae Toolbox database (Wang *et al.*, 2014), and were BLAST searched against Phytozome's version 2.2 of the wheat genome and identified candidate genes located ±250 kb proximal to each identified marker. Candidate genes of interest were selected based on the criteria of close proximity to the SNP, and possible involvement in the regulation of root development.

Data and statistical code availability

All trait data, GEMMA output, and R analysis scripts necessary for doing the statistical analysis and plotting are available at https://doi.org/10.5281/zenodo.4247894 (Guo *et al.*, 2020b).

Results

Variations of root respiratory and architectural traits

Shoot dry weight (SDW), RDW, TDW, TRR, SRL, L-to-A_L, ASA, L-to-A_V, PC2, PC3, PC4, and PC7 exhibited normal distribution. Near normal distributions were observed for other root traits (Fig. S1). The root traits with more than 5-fold variation between maximum and minimum values in the wheat population were SRR_L, TRL, LRL, LRV, LSA, and BP. 3.2-fold and 2.2-fold variations were also observed in SRR_M and SRL in the wheat population, respectively. Broad-sense heritabilities ranged from 0.25 to 0.57 for the 25 traits (Table 1). The respiration residual, SRR_R, of a multiple regression fit (Figure 2a) that accounts for respiration not explained by root system architecture, had a heritability of 0.44. The maximum heritability was observed for SDW (0.57). The root traits with heritabilities greater than 0.50 were SRL, BP, and AvgD. Many strong correlations were observed among traits. Total root respiration had correlation values greater than 0.50 with RDW and TDW. Interestingly, specific root respiratory traits (SRR_L and SRR_M) had significant negative correlations with shoot, root, and total dry weight (Figure 2b, Figure 3).

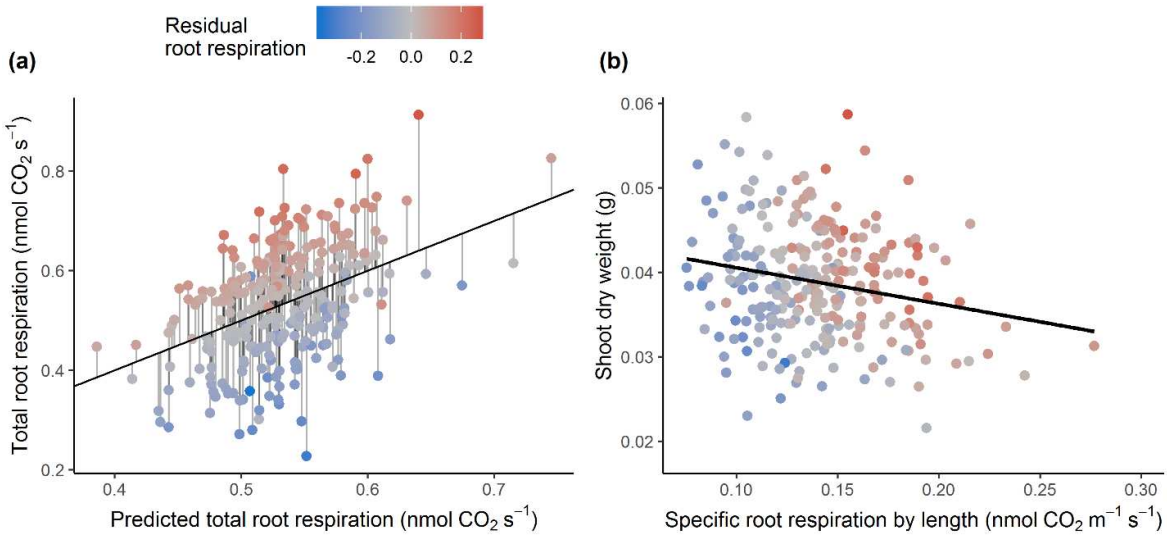

Figure 2 (a) The relationship between predicted total root respiration and total root respiration, and deviations from the relationship results in new trait SRR_R, (b) Regression between specific root respiration by length and shoot dry weight.

Table 1. Summary statistics and units for shoot dry weight, total dry weight, and the 24 root traits characterized in this study.

Trait	Abbreviation	Unit	Mean	Min	Max	H^2
Shoot dry weight	SDW	g	0.039	0.018	0.059	0.57
Total dry weight	TDW	g	0.053	0.024	0.080	0.51
Root dry weight	RDW	g	0.014	0.006	0.022	0.39
Total root respiration	TRR	nmol CO_2 s^{-1}	0.54	0.23	0.91	0.42
SRR per root length	SRR_L	nmol CO_2 s^{-1} m^{-1}	0.14	0.04	0.34	0.48
SRR per root mass	SRR_M	nmol CO_2 s^{-1} g^{-1}	39.86	23.32	74.79	0.32
SRR residual	SRR_R	nmol CO_2 s^{-1}	-0.0039	-0.3623	0.27	0.44
Specific root length	SRL	m g^{-1}	299.7	182.21	398.36	0.55
Root mass fraction	RMF	%	26.48	19.05	36.17	0.43
Total root length	TRL	mm	4125.91	1315.65	7861.83	0.47
Axial root length	ARL	mm	1456.2	655.59	2537.42	0.48
Lateral root length	LRL	mm	2669.71	660.06	5494.75	0.48
Lateral-to-axial root length ratio	L-to-A_L	mm mm^{-1}	1.82	0.83	2.66	0.48
Total root volume	TRV	mm^3	329.49	135.78	610.24	0.45
Axial root volume	ARV	mm^3	243.9	113.64	459.5	0.46
Lateral root volume	LRV	mm^3	85.59	22.15	164.09	0.40
Lateral-to-axial root volume ratio	L-to-A_V	mm^3 mm^{-3}	0.36	0.17	0.53	0.45
Total root surface area	TSA	mm^2	3680.62	1348.64	6477.28	0.45
Axial root surface area	ASA	mm^3	2034.03	934.42	3639.73	0.47
Lateral root surface area	LSA	mm^3	1646.59	414.22	3266.23	0.44
Average root diameter	AvgD	mm	0.29	0.25	0.37	0.53
Number of root tips	Tip	n	399.61	161.67	710	0.40
Number of branch points	BP	n	931.66	283	1992.5	0.54
Branching frequency	BF	n mm^{-1}	0.22	0.18	0.31	0.45
Branching density	BD	n cm^{-1}	2.81	1.75	5.83	0.25
Root tissue density	RTD	g cm^{-3}	0.04	0.03	0.06	0.30

H^2, broad-sense heritability.

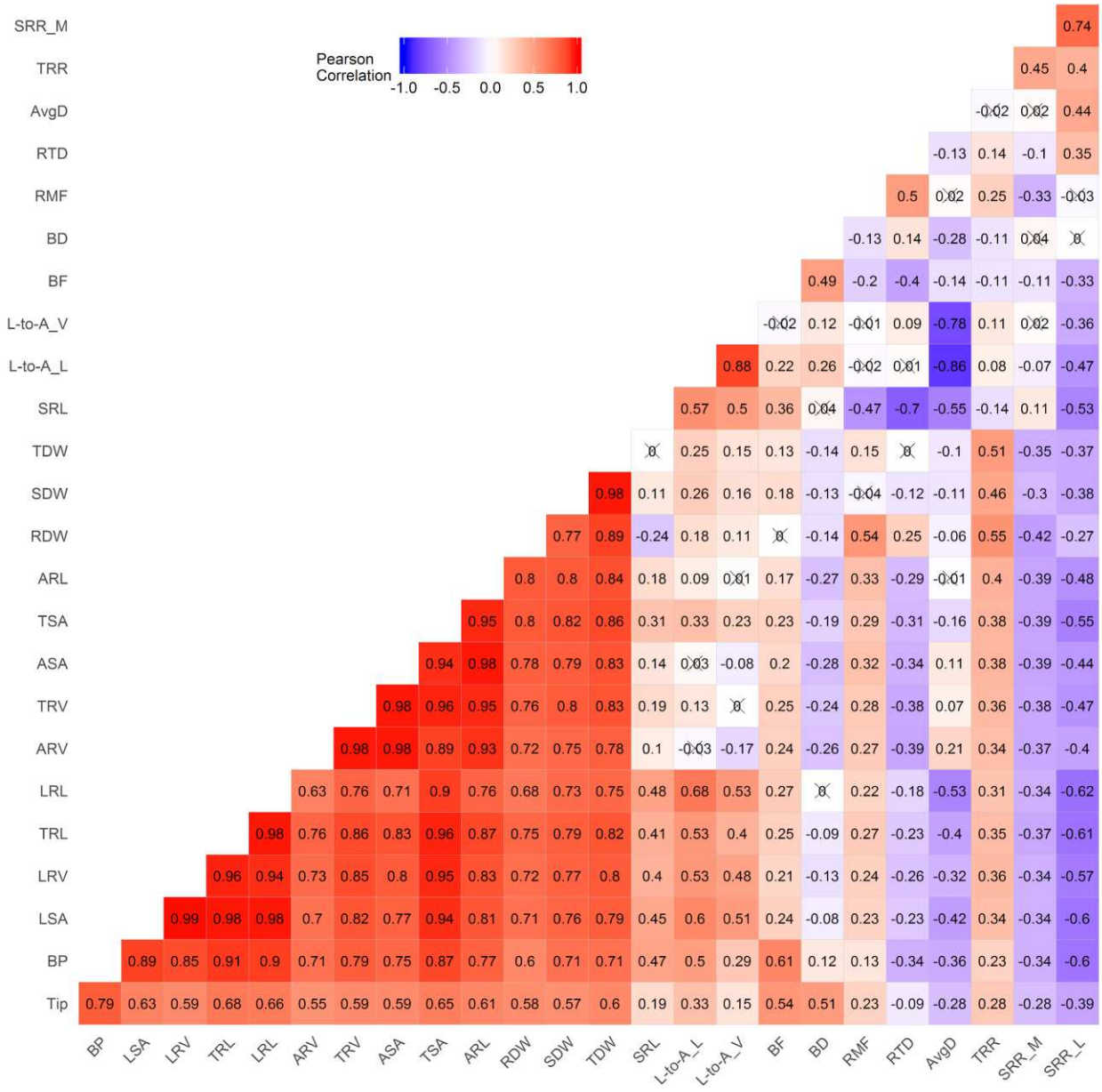

Figure 3 Pairwise Pearson correlation of selected traits of TCAP winter wheat seedlings. The number represents the correlation values. Value marked with symbol × means correlation is not significant at p = 0.05. Bright red to bright blue indicates highly positive to highly negative correlations, respectively. Trait abbreviations are as in Table 1.

Principal component analysis of the traits was conducted to further identify the major linear trait combinations that maximize the multivariate variation, and the first ten PCs collectively explained 98.8% of the total variance. PC1, PC2, PC3, and PC4 explained 49.9%, 17.5%, 9.3%, and 7.7% of the total variance, respectively (Figure 4a). Plant size-related traits

including TSA, TRL, TRV, TDW, RDW, and SDW had important contributions (>5%) to PC1. In contrast, PC2 was largely driven by two construction cost related traits AvgD and SRL, which had contributions of 18% and 15%, respectively (Figure 4b). Traits with greater than 7% contributions to PC3 were the construction cost trait RTD (22%), three root respiration traits (TRR, SRR_L, and SRR_M), and branching trait BF (14%). PC4 was predominantly driven by SRR_M and SRR_L that represent metabolic costs, which had contributions of 24% and 14% to the component, respectively (Figure 4c).

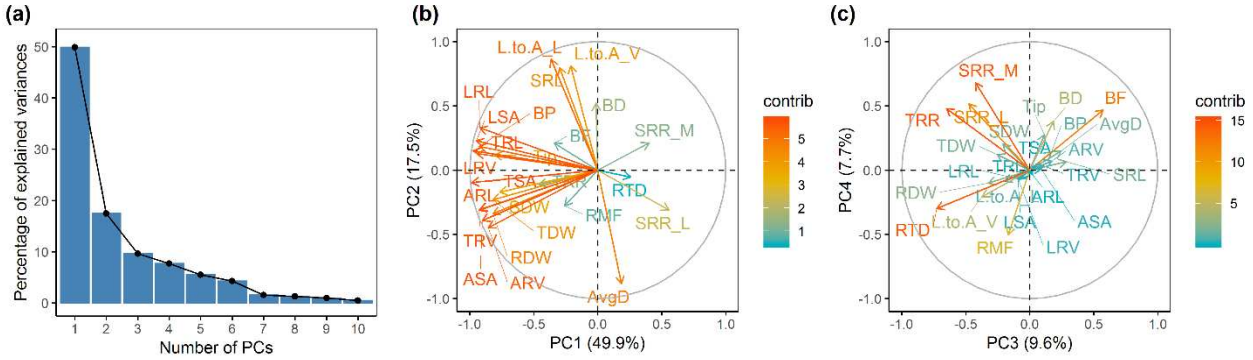

Figure 4 (a) Scree graph showing the percentage of variance explained by each of the first 10 principal components, PCA variable contribution plots showing the (b) first and second PCs and (c) third and fourth PCs, where vectors indicate relative weightings of the variables. Trait abbreviations are as in Table 1.

Multiple linear regression partitions respiration among root tissue types

Multiple linear regression analysis was employed to determine the respective contributions of lateral root tip, lateral root axis, and toal axial root volumes to total root respiration, and to provide the SRR_R trait. The resulting model (p < 2.2e-16) explains 14.5% of the variation in total root respiration. Axial root volume, lateral root volume, and lateral root tip volume were all significant explanatory variables (p = 0.001, 1.37e-05, and 0.033, respectively). The average specific root respiration rate on a volume basis of lateral root tips was 30.5 and 8.1 times the rates of axial roots and lateral roots, respectively, as determined from comparing slopes in the model. The residuals represent respiration not accounted for by average tissue dependencies within the diversity panel, which we hypothesized to have a genetic component.

Trait correlation network

In addition to the correlation analyses, a network analysis based on a Gaussian graphical model was performed to account for the conditional dependencies between the investigated

traits. The traits exhibiting outdegree greater than 2.0 were AvgD, RTD, ARL, SRR_M, and SRL in descending order (Table S1). Average root diameter showed the highest betweenness, connecting a root branching subnetwork via ARL, and a biomass subnetwork via RMF. SRL also exhibited a high betweenness, by connecting other groups of traits belonging to root respiration, biomass, root morphology, and topology. Consistent with Pearson correlation analysis, SRR_M was weakly connected with root dry weight, total dry weight, and RMF. SRL was negatively and positively correlated with SRR_L and SRR_M, respectively (Figure 5). In contrast to the Pearson correlation analysis (Figure 3), no direct network connection was observed between shoot dry weight and root respiratory and architectural traits (Figure 5).

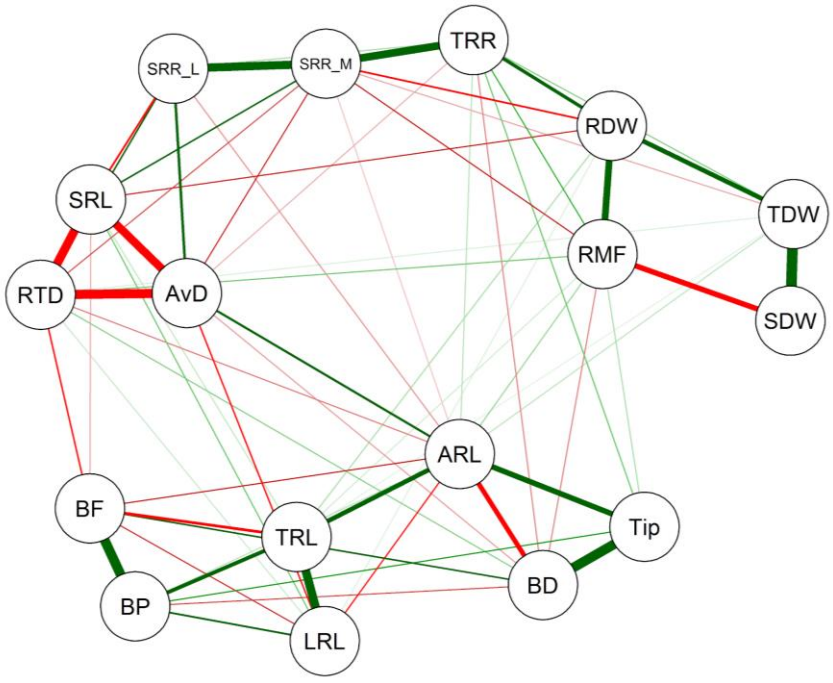

Figure 5 Trait correlation network constructed from Gaussian graphical model. Red and green edges show negative and positive correlations, respectively. Cutoff was set at 0.15. Trait abbreviations are as in Table 1.

Genome-wide association analysis

Multi-trait GWAS on the six sets of traits identified 140 SNPs while the single-trait GWAS of 25 traits identified 234 significantly associated SNPs ($-\log_{10} P = 3.5$). GWAS based on the first 10 PCs identified 79 SNPs that passed the $-\log_{10}P$ of 3.5, and the majority of these detected SNPs were associated with PC1, PC2 or PC9 (Figure 6a, Table S2). Sixty-nine percent of the significantly associated SNPs in multi-trait approach and 56% of the SNPs in PC-GWAS

were represented in the single-trait GWAS (Figure 6). Overall, multi-trait GWAS and PC-GWAS identified 77 additional, unique SNPs that were not uncovered by the 25 univariate analyses (Figure 6a, Figure S2).

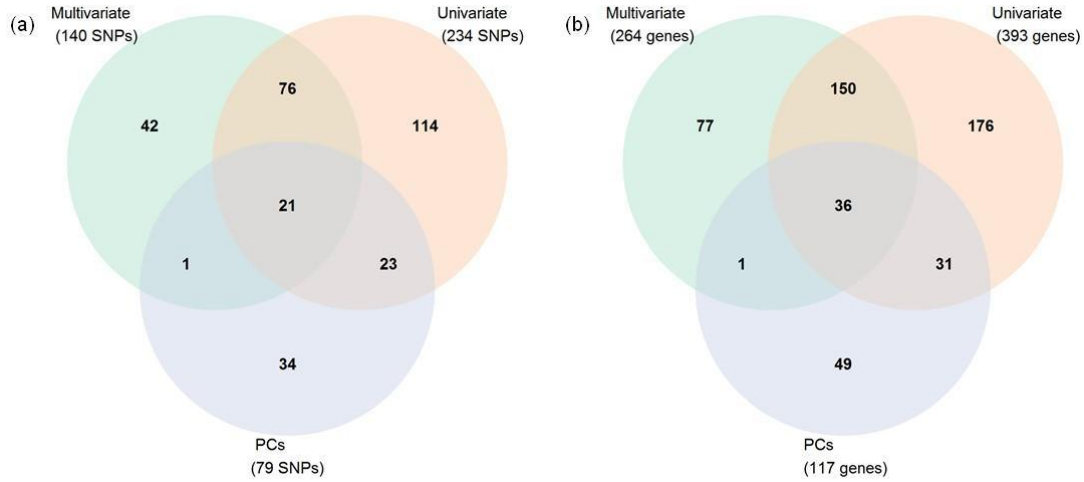

Figure 6 Venn diagram of (a) associated SNPs cutoff set at $-\log_{10}P=3.5$, (b) genes identified using cutoff set at $-\log_{10}P= 3.5$ comparing significantly univariate of mean 25 traits, univariate analyses of 10 principal components (PCs), and multivariate of 6 trait combinations.

Four significant markers associated with SRR_M were identified on chromosomes 1B, 4B and 4D (Figure 7a). There were no genes underlying the top two largest $-\log_{10}P$ signals on chromosomes 1B and 4B, while the third largest $-\log_{10}P$ signal (IWA430) on chromosome 4D was encoding for four underlying proteolysis genes involved in cellular protein catabolic process (Table S3). Seven significant markers associated with SRR_L were identified on chromosomes 4B and 5A. The marker (Excalibur_c100336_106) with the largest $-\log_{10}P$ signal on chromosome 4B, which co-associated with SRR_M, had no known underlying gene. Six genes underlying the next two largest $-\log_{10}P$ signals on chromosome 5A were annotated with functions as ATP binding, protein binding, and protein kinase activity (Table S3). Three additional significant markers associated with SRR_R were detected on chromosomes 1A and 1B (Table 2). Three genes underlying the largest $-\log_{10}P$ signal (Kukri_c10453_875) on chromosome 1A were associated with processes of DNA transcription regulation (Table S3). There were no genes underlying the other two markers. Multi-trait GWAS for root respiration identified 20 additional markers on chromosomes 1A, 1B, 2B, 3D, 4A, 4B, 5B, 6A, and 7A (Figure 7a). There were no known genes underlying the largest $-\log_{10}P$ signal Excalibur_c5139_198 on chromosome 1A, and four genes underlying the following two largest -

$log_{10}P$ signals on chromosomes 1A and 1B were annotated with functions as protein kinase activity and ADP binding (Table S3).

Ten significant markers associated with single-trait SRL were identified on chromosomes 2A (9 markers) and 7A, and seventeen genes underlying the top three largest $–log_{10}P$ signals on chromosome 2A and 7A have functions related to protein binding, calcium ion binding, polysaccharide binding, and ATP binding (Figure 7b, Table S3). Five significant markers associated with single-trait AvgD were identified on chromosomes 6B, 7A, and 7B. Only one of the top three largest $–log_{10}P$ signals on chromosome 7Ahad three underlying genes, which were annotated with function as protein binding. Seven significant markers associated with single-trait RTD were identified on chromosomes 1B, 1D, and 7A, and eight genes underlying the top three largest $–log_{10}P$ signals on chromosomes 1B, 1D, and 7A were annotated as zinc finger CW-type coiled-coil domain protein and integral membrane Yip1 family protein. Multi-trait GWAS for root construction identified eight markers on chromosomes 1A, 1B, 2B, 3B, and 7A, with one marker (GENE-0249_161) on 1B co-associated with single-trait RTD, and another marker (RAC875_c63889_486) on 7A co-associated with single-trait SRL (Table 2). Eight genes underlying the top three largest $–log_{10}P$ signals on chromosomes 1B, 2B, and 3B were annotated as regulators of VPS4 activity protein-related and potassium ion transmembrane transport (Table S3).

Thirty-four significant markers associated with single-trait BF were identified on chromosomes 1A, 2A, 2D, 6A, and 6D, and seven genes underlying the top two largest $–log_{10}P$ signals on chromosome 1A involved in biological processes such as oxidation-reduction, steroid biosynthetic process, and DNA-binding process. We detected 134 markers for single-trait BP on chromosomes 1A, 1D, 2A, 2D, 5A, 5B, and the top three largest $–log_{10}P$ signals and underlying nine genes were all observed on chromosome 1D, which also co-associated with multi-trait root topology. Three significant marker associations were detected for single-trait branching density on chromosomes 2D, 4B, and 5A (Figure 7c), and five genes underlying the three markers had annotations indicating involvement in oxidation-reduction biological processes. Multi-trait GWAS for root topology identified 84 significant markers, with 80 markers co-associated with single-trait BF or BP (Figure 7c). Significant marker associations and underlying genes were also detected for multi-trait biomass, multi-trait allocation, multi-trait morphology, for all PC-traits except PC8, and for the other single traits (Figure 6, Figure S2, Table S3).

Table 2. Subset of significant SNP markers identified from multi-trait GWAS and univariate GWAS of single-trait by selecting top three SNPs of each trait.

Trait	Model	Markers	Chr	MAF	p value
SRR_M	Univariate	Excalibur_c100336_106	4B	0.110	1.91E-05
SRR_M	Univariate	IAAV5776	1B	0.056	9.95E-05
SRR_M	Univariate	IWA430	4D	0.438	2.11E-04
SRR_L	Univariate	Excalibur_c100336_106	4B	0.110	1.70E-05
SRR_L	Univariate	CAP12_c956_61	5A	0.112	2.04E-04
SRR_L	Univariate	BS00066434_51	5A	0.146	2.19E-04
SRR_R	Univariate	Kukri_c10453_875	1A	0.281	7.51E-05
SRR_R	Univariate	IWA6965	1B	0.064	9.86E-05
SRR_R	Univariate	RAC875_c42206_305	1B	0.064	9.86E-05
Respiration	Multivariate	Excalibur_c5139_198	1A	0.213	5.69E-06
Respiration	Multivariate	tplb0048b10_1365	1B	0.064	4.35E-05
Respiration	Multivariate	Ex_c4876_1221	1A	0.248	9.36E-05
SRL	Univariate	RAC875_c63889_486	7A	0.202	7.58E-05
SRL	Univariate	GENE-1220_457	2A	0.064	1.29E-04
SRL	Univariate	RFL_Contig5917_2369	2A	0.071	1.73E-04
AvgD	Univariate	IWA7907	7B	0.190	1.95E-04
AvgD	Univariate	IWA4438	7A	0.083	1.97E-04
AvgD	Univariate	Tdurum_contig61864_1352	7A	0.082	2.03E-04
RTD	Univariate	GENE-0249_161	1B	0.272	6.84E-05
RTD	Univariate	IWA614	7A	0.277	1.97E-04
RTD	Univariate	Kukri_c20062_389	1D	0.165	2.06E-04
Construction	Multivariate	BS00082644_51	3B	0.247	4.91E-05
Construction	Multivariate	GENE-0249_161	1B	0.272	1.65E-04
Construction	Multivariate	IWA6076	2B	0.273	1.72E-04
BF	Univariate	CAP7_c1083_283	1A	0.140	1.74E-05
BF	Univariate	Kukri_c29121_226	1A	0.140	1.98E-05
BF	Univariate	Kukri_c53935_265	1A	0.136	3.47E-05
BP	Univariate	IWA1464	1D	0.147	6.00E-07
BP	Univariate	BS00032149_51	1D	0.133	7.39E-07
BP	Univariate	IWA2164	1D	0.150	1.31E-06
BD	Univariate	Tdurum_contig49608_1185	4B	0.143	1.59E-04
BD	Univariate	BS00063973_51	5A	0.404	2.63E-04
BD	Univariate	Excalibur_c33173_557	2D	0.205	2.91E-04
Topology	Multivariate	BS00032149_51	1D	0.133	6.15E-06
Topology	Multivariate	IWA1464	1D	0.147	6.95E-06
Topology	Multivariate	IWA2164	1D	0.150	1.74E-05

Chr, Chromosome; MAF, minor allele frequency.

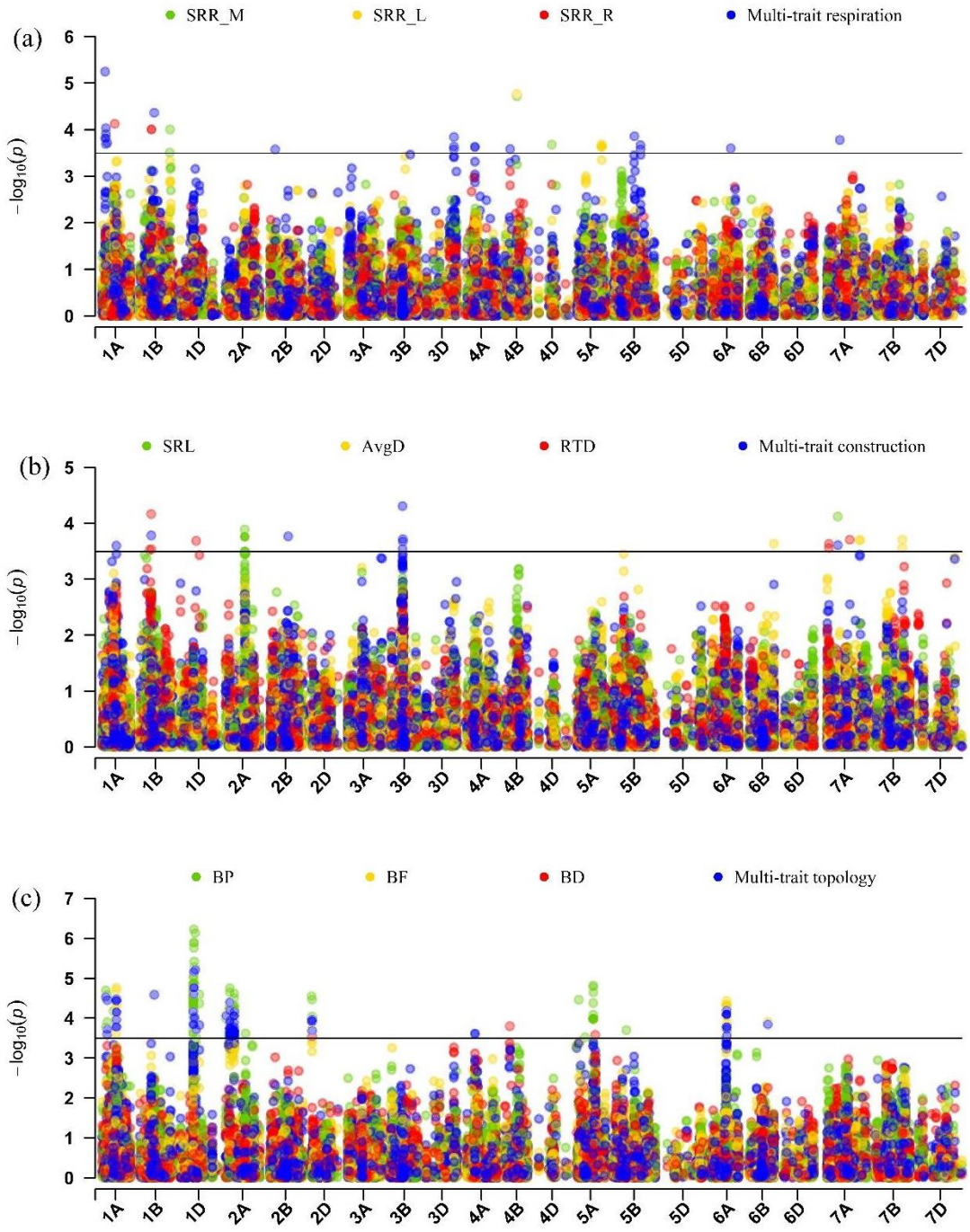

Figure 7 Manhattan plot of GWAS conducted on traits (a) SRR by mass, SRR by length, residuals of total respiration vs volume of different segments, and multi-trait combination for root respiration, (b) SRL, AvgD, RTD, and multi-trait combination for root construction, (c) BP, BF, BD, and multi-trait combination for root topology of TCAP wheat population. Each dot represents a SNP. The horizontal black line indicates the threshold of significance at - $\log_{10}$P = 3.5. Trait abbreviations are as in Table 1.

Discussion

Reducing the metabolic and construction carbon costs of roots has become a realistic engineering strategy for crop breeding to increase yield and promote plant growth (Lynch, 2013; Lynch, 2018; Amthor *et al.*, 2019). However, the genetic and functional basis of root respiration traits still lags behind architectural root traits. Scaling up the throughput of root respiration phenotyping will strengthen functional phenomics greatly by increasing statistical power and enabling genetic mapping (York, 2019). The platform we developed facilitates high-throughput phenotyping of root respiration, with integration of cost-effective equipment and an R script for data processing, and allowed throughput of about 25 samples person^{-1} hour^{-1}. The use of a bead bath for controlling temperature avoids the risk found when using a water bath of water entering the respiration chamber and contaminating the gas analyzer. We observed 8.5-fold variation for SRR_L and 3.2-fold variation for SRR_M in the wheat panel. In previous work, root respiration was measured mostly using single root segments (Poorter *et al.*, 1991; Strock *et al.*, 2018), and there was little information about how different root types impact respiration of whole root systems. Considering the difficulty of separating different root tissue segments from whole root systems for maintaining high-throughput, multiple linear regression was used to predict the contributions of root tissue types to total root respiration of wheat seedlings on average within the panel. We found that the lateral root tips had much greater respiration than axial root tissue or lateral root axis tissue($\leq$ 0.3 mm), which supports findings in woody plants that root tip meristems consume about 15 times more O_2 than the rest of the root system (Mancuso & Boselli, 2002; Aguilar *et al.*, 2003; Burton *et al.*, 2012).

Correlation network analyses have been widely used in biology and social sciences to capture causality and precursor/product relationship patterns in functional traits. Despite the elegance of this approach, only a few studies applied network theory to plant root traits (Poorter *et al.*, 2014; Messier *et al.*, 2017; Carlson *et al.*, 2019; Kleyer *et al.*, 2019). In addition to root dry weight, SRL, and average diameter, SRR_M, which is rarely used in functional trait analysis, was identified as one of the hub traits and had substantial effects on the plant phenotype as a whole. Consistent with previous work, SRL correlated with root dry weight, root diameter, branching, and root tissue density (Reich, 2014; Kramer-Walter *et al.*, 2016). In addition, we found that SRL also can be an indicator of root respiration on either a mass or length basis. Shoot biomass only had a strong positive correlation with total biomass and a negative correlation with

root mass fraction in the network, which may indicate that the formation of wheat seedling shoot biomass was mostly independent, and also indicates that reducing or otherwise optimizing the allocation of resources to the root could be a strategy to improve shoot growth (Guo & York, 2019). Counterintuitively, driving shoot growth with such a strategy may actually maintain root mass and total metabolic burden, or even increase these total costs, but with less proportion relative to the shoot. This framework of carbon use efficiency represents an untapped positive feedback loop for plant growth. Interestingly, network, principal component, and regression analyses all showed that SRR_M was negatively correlated with total dry weight, suggesting that reducing respiratory carbon could potentially increase whole-plant growth (Lynch, 2015; Amthor *et al.*, 2019).

Multi-trait GWAS has recently gained more attention because it often boosts the power to detect SNPs and assesses the full spectrum of traits that are affected by trait-associated variants (Porter & O'Reilly, 2017), which can be particularly useful for challenging physiological traits (Chhetri *et al.*, 2019). Combining traits related to respiration, multi-trait association analysis identified 20 unique significant associations while single-trait GWAS detected 13 unique significant associations for all SRR traits. The findings potentially reveal the pleiotropic effects of genes near significantly associated SNPs on root respiration. The marker tplb0048b10_1365, the second-largest -$\log_{10}$P signal associated with multi-trait root respiration, was reported to be associated with nitrogen deficiency tolerance in wheat seedlings (Ren *et al.*, 2018). Multiple annotated genes underlying significant SRR_L and SRR_M associated SNPs are annotated with functions in protein catabolism, protein binding, ADP, and ATP binding, which are related to cellular respiration (Araújo *et al.*, 2011), root meristem activity (Xu *et al.*, 2017) or root senescence (Liu *et al.*, 2019).

GWAS for root architectural traits have gained increasing attention in wheat, and several QTL/genes in wheat have been found to associate with root architectural and morphological traits such as root length, root number, and root diameter across the genome (Maccaferri *et al.*, 2016; Ayalew *et al.*, 2018; Beyer *et al.*, 2019). Specific root length (SRL), AvgD, and RTD are important components of the root economic spectrum because they potentially provide information about root morphology and construction costs (Kramer-Walter *et al.*, 2016; McCormack *et al.*, 2017). Multiple genes underlying associated significant SNPs were identified as zinc finger protein, cytochrome p450 family member, and haloacid dehalogenase-like

hydrolase family protein, which all play important roles in controlling wheat root growth and development (Kulkarni *et al.*, 2017; Li & Wei, 2020). Multiple genes underlying two markers (Kukri_c24648_262 and Kukri_c5113_1082), which were co-associated with TRL, LRL, TRV, LRV, TSA, LSA, BP, PC1, and multi-trait allocation and topology (Table S3), were annotated as a nucleoporin autopeptidase domain containing protein. Those genes may play distinct roles in nuclear transport and root elongation (Parry, 2014).

Root branching is a necessary developmental process for increasing the number of growing tips and defining the distribution of their meristem sizes (Pagès, 2014), with a large metabolic cost. Root branching was critical for plant survival and performance under abiotic conditions (Schneider *et al.*, 2020). Two genes (Traes_1AL_9CC946A58 and Traes_1DL_7EF27C52F) underlying the largest -$\log_{10}$P signal of BF were annotated as being involved in steroid biosynthesis, which may play a role in interacting with auxin signaling to promote lateral root growth (Vriet *et al.*, 2012; Wang *et al.*, 2018). Four genes underlying the marker BS00013534_51, which was co-associated with BF, BP, and multi-trait topology, were annotated as encoding protein kinase activity in wheat and threonine-protein kinase receptor precursor in rice. Interestingly, different genes with similar functions were found playing fundamental roles in lateral root formation and development (Atkinson *et al.*, 2014; Yu *et al.*, 2016; Pan *et al.*, 2020). Three candidate genes underlying single-trait branching frequency and multi-trait topology co-associated SNP (tplb0025i05_1836) were annotated as being involved in the activity of Rho guanine nucleotide exchange factors. Rho family members are well known as regulators of extracellular stimulus-dependent signaling pathways that affect gene expression, cell proliferation, actin cytoskeleton, cell cycle progression, and cell polarity (Berken & Wittinghofer, 2008).

A recent review outlined the emerging possibilities for targeted reducing unnecessary carbon loss for increasing yields (Amthor *et al.*, 2019), which was further supported by new simulation results indicating that substantial gains could be made by targeting plant respiration (Holland *et al.*, 2019). Therefore, an optimal root system will conform to economic cost-benefit analysis where the cost increment of allocation to the root system equals the benefit increment, measured as nutrient and water capture, or marginal photosynthesis (Bloom *et al.*, 1985). Recent work from the RIPE project has also shown it's possible to increase photosynthesis by reducing photorespiration (South *et al.*, 2019) and increasing photosynthetic induction (Acevedo-Siaca *et*

al., 2020). We propose that combining strategies that increase photosynthesis and decrease 'luxury' root respiration could have synergistic and compounding influences on plant growth. The root economics space discussed above provides a useful framework for this strategy.

Conclusions

We developed a high-throughput platform for measuring multiple traits within the root economics space, including root respiration and specific root length which are aspects of root metabolic and construction costs, respectively. Substantial, heritable variation exists within wheat, providing further evidence for intraspecific economics spectra. Employing the functional phenomics approach allowed leveraging genetic and phenotypic diversity to infer the increased contribution of lateral root tips to respiration, the negative relation of SRR to seedling mass, and network analysis that identified hub traits. Genome-wide association studies for the univariate traits uncovered several underlying genetic regions, while multivariate and PCA-based GWAS provided increased power to detect genetics of the root economics space itself for the first time to our knowledge. The SNPs associated with the traits may be useful for marker-assisted breeding. Candidate genes underlying significant SNPs associated with root respiratory, construction, and topology traits will require further research for reducing respiratory carbon loss and construction costs. We provide evidence that combining functional phenomics methods and trait economic theory has substantial potential to advance plant biology and crop breeding.

Acknowledgements

This research was supported by the Noble Research Institute, LLC and the Samuel Roberts Noble Foundation. The authors wish to acknowledge David McSweeney and Karen Hartman of Greenhouse Core Facility for assistance provided during the experiment, Nick Krom of Scientific Computing Department for assistance with BLAST searches for candidate genes, and contributions from Yaxin Ge, Michael Cloyde, Na Ding, Xinji Zhang, Guangming Li, and Wangqi Huang for data acquisition and sampling.

Author contributions

HG and LMY designed the experiments. X-FM provided the germplasm and expertise for genetic analysis. HG, AS, KD, and LMY conducted experiments. HG, MG, AS, KD, and LMY developed the respiration measurement protocol and R script for root respiration analysis. HG,

AS, KD, HA, and LMY analyzed the experimental data. HG and LMY wrote the first draft of the manuscript, all authors made revisions, and all approved the final version.

ORCID

Haichao Guo https://orcid.org/0000-0003-2778-1188

Habtamu Ayalew https://orcid.org/0000-0002-4778-9008

Anand Seethepalli https://orcid.org/0000-0003-0937-9128

Kundan Dhakal https://orcid.org/0000-0001-5827-378X

Marcus Griffiths https://orcid.org/0000-0003-2349-8967

Xue-Feng Ma https://orcid.org/0000-0002-0942-9116

Larry M. York https://orcid.org/0000-0002-1995-9479

References

Acevedo-Siaca LG, Coe R, Wang Y, Kromdijk J, Quick WP, Long SP. 2020. Variation in photosynthetic induction between rice accessions and its potential for improving productivity. *New Phytologist* **227**: 1097-1108.

Aguilar E, Turner D, Gibbs D, Armstrong W, Sivasithamparam K. 2003. Oxygen distribution and movement, respiration and nutrient loading in banana roots (Musa spp. L.) subjected to aerated and oxygen-depleted environments. *Plant and Soil* **253**(1): 91-102.

Amthor J. 2000. The McCree–de Wit–Penning de Vries–Thornley Respiration Paradigms: 30 Years Later. *Annals of Botany* **86**(1): 1-20.

Amthor JS, Bar-Even A, Hanson AD, Millar AH, Stitt M, Sweetlove LJ, Tyerman SD. 2019. Engineering Strategies to Boost Crop Productivity by Cutting Respiratory Carbon Loss. *The Plant Cell* **31**(2): 297-314.

Araújo WL, Tohge T, Ishizaki K, Leaver CJ, Fernie AR. 2011. Protein degradation–an alternative respiratory substrate for stressed plants. *Trends in Plant Science* **16**(9): 489-498.

Atkinson JA, Rasmussen A, Traini R, Voß U, Sturrock C, Mooney SJ, Wells DM, Bennett MJ. 2014. Branching out in roots: uncovering form, function, and regulation. *Plant Physiology* **166**(2): 538-550.

Atkinson JA, Wingen LU, Griffiths M, Pound MP, Gaju O, Foulkes MJ, Le Gouis J, Griffiths S, Bennett MJ, King J. 2015. Phenotyping pipeline reveals major seedling root growth QTL in hexaploid wheat. *Journal of Experimental Botany* **66**(8): 2283-2292.

Ayalew H, Liu H, Borner A, Kobiljski B, Liu C, Yan G. 2018. Genome-Wide Association Mapping of Major Root Length QTLs Under PEG Induced Water Stress in Wheat. *Frontiers in Plant Science* **9**: 1759.

Bai C, Liang Y, Hawkesford MJ. 2013. Identification of QTLs associated with seedling root traits and their correlation with plant height in wheat. *Journal of Experimental Botany* **64**(6): 1745-1753.

Bates D, Maechler M, Bolker B, Walker S, Christensen RHB, Singmann H, Dai B 2014. lme4: Linear mixed-effects models using Eigen and S4 (Version 1.1-7).

Ben-Noah I, Friedman SP. 2018. Review and Evaluation of Root Respiration and of Natural and Agricultural Processes of Soil Aeration. *Vadose Zone Journal* **17**(1).

Bergmann J, Weigelt A, van der Plas F, Laughlin DC, Kuyper TW, Guerrero-Ramirez N, Valverde-Barrantes OJ, Bruelheide H, Freschet GT, Iversen CM, et al. 2020. The fungal collaboration gradient dominates the root economics space in plants. *Science Advances* **6**(27): eaba3756.

Berken A, Wittinghofer A. 2008. Structure and function of Rho-type molecular switches in plants. *Plant Physiology and Biochemistry* **46**(3): 380-393.

Beyer S, Daba S, Tyagi P, Bockelman H, Brown-Guedira G, Iwgsc, Mohammadi M. 2019. Loci and candidate genes controlling root traits in wheat seedlings-a wheat root GWAS. *Funct Integr Genomics* **19**(1): 91-107.

Bloom AJ, Chapin III FS, Mooney HA. 1985. Resource limitation in plants-an economic analogy. *Annual review of Ecology and Systematics* **16**(1): 363-392.

Burton AJ, Jarvey JC, Jarvi MP, Zak DR, Pregitzer KS. 2012. Chronic N deposition alters root respiration - tissue N relationship in northern hardwood forests. *Global Change Biology* **18**(1): 258-266.

Carlson MO, Montilla-Bascon G, Hoekenga OA, Tinker NA, Poland J, Baseggio M, Sorrells ME, Jannink JL, Gore MA, Yeats TH. 2019. Multivariate Genome-Wide Association Analyses Reveal the Genetic Basis of Seed Fatty Acid Composition in Oat (Avena sativa L.). *G3 (Bethesda)* **9**(9): 2963-2975.

Chhetri HB, Macaya-Sanz D, Kainer D, Biswal AK, Evans LM, Chen JG, Collins C, Hunt K, Mohanty SS, Rosenstiel T, et al. 2019. Multitrait genome-wide association analysis of Populus trichocarpa identifies key polymorphisms controlling morphological and physiological traits. *New Phytologist* **223**(1): 293-309.

Cormier F, Foulkes J, Hirel B, Gouache D, Moënne-Loccoz Y, Le Gouis J, Ordon F. 2016. Breeding for increased nitrogen-use efficiency: a review for wheat (T. aestivumL.). *Plant Breeding* **135**(3): 255-278.

Dorion S, Clendenning A, Rivoal J. 2017. Engineering the expression level of cytosolic nucleoside diphosphate kinase in transgenic Solanum tuberosum roots alters growth, respiration and carbon metabolism. *Plant J* **89**(5): 914-926.

Ellis JG, Lagudah ES, Spielmeyer W, Dodds PN. 2014. The past, present and future of breeding rust resistant wheat. *Frontiers in Plant Science* **5**: 641.

Epskamp S, Cramer AO, Waldorp LJ, Schmittmann VD, Borsboom D. 2012. qgraph: Network visualizations of relationships in psychometric data. *Journal of Statistical Software* **48**(4): 1-18.

Falconer D, Mackay T. 1996. Introduction to quantitative genetics. 1996. *Harlow, Essex, UK: Longmans Green* **3**.

Florez-Sarasa I, Fernie AR, Gupta KJ. 2020. Does the alternative respiratory pathway offer protection against the adverse effects resulting from climate change? *Journal of Experimental Botany* **71**(2): 465-469.

Guo H, Ayalew H, Seethepalli A, Dhakal K, Griffiths M, Ma X-F, York LM 2020b. Data and statistical analysis scripts for manuscript on high-throughput phenotyping of root economics in wheat. *Zenodo. DOI: 10.5281/zenodo.4247894*.

Guo H, Griffiths M, Seethepalli A, Dhakal K, York LM 2020a. Protocol and data analysis scripts for high-throughput phenotyping of specific root respiration. *Zenodo. DOI: 10.5281/zenodo.4247873*.

Guo H, York LM. 2019. Maize with fewer nodal roots allocates mass to more lateral and deep roots that improve nitrogen uptake and shoot growth. *J Exp Bot* **70**(19): 5299-5309.

Hamada A, Nitta M, Nasuda S, Kato K, Fujita M, Matsunaka H, Okumoto Y. 2012. Novel QTLs for growth angle of seminal roots in wheat (Triticum aestivum L.). *Plant and Soil* **354**(1-2): 395-405.

Hawkesford MJ, Griffiths S. 2019. Exploiting genetic variation in nitrogen use efficiency for cereal crop improvement. *Curr Opin Plant Biol* **49**: 35-42.

Holland BL, Monk NA, Clayton RH, Osborne CP. 2019. A theoretical analysis of how plant growth is limited by carbon allocation strategies and respiration. *in silico Plants* **1**(1): diz004.

Johnson I. 1983. Nitrate uptake and respiration in roots and shoots: a model. *Physiologia Plantarum* **58**(2): 145-147.

Kassambara A, Mundt F. 2017. Package 'factoextra'. *Extract and visualize the results of multivariate data analyses* **76**.

Kleyer M, Trinogga J, Cebrián‐Piqueras MA, Trenkamp A, Fløjgaard C, Ejrnæs R, Bouma TJ, Minden V, Maier M, Mantilla‐Contreras J. 2019. Trait correlation

network analysis identifies biomass allocation traits and stem specific length as hub traits in herbaceous perennial plants. *Journal of Ecology* **107**(2): 829-842.

Kramer-Walter KR, Bellingham PJ, Millar TR, Smissen RD, Richardson SJ, Laughlin DC. 2016. Root traits are multidimensional: specific root length is independent from root tissue density and the plant economic spectrum. *Journal of Ecology* **104**(5): 1299-1310.

Krumsiek J, Suhre K, Illig T, Adamski J, Theis FJ. 2011. Gaussian graphical modeling reconstructs pathway reactions from high-throughput metabolomics data. *BMC systems biology* **5**(1): 21.

Kulkarni M, Soolanayakanahally R, Ogawa S, Uga Y, Selvaraj MG, Kagale S. 2017. Drought response in wheat: key genes and regulatory mechanisms controlling root system architecture and transpiration efficiency. *Frontiers in Chemistry* **5**: 106.

Lambers H, Atkin OK, Millenaar FF. 1996. Respiratory patterns in roots in relation to their functioning. *Plant roots. The hidden half* **3**: 521-552.

Li Y, Wei K. 2020. Comparative functional genomics analysis of cytochrome P450 gene superfamily in wheat and maize. *BMC plant biology* **20**(1): 1-22.

Liu Z, Marella CB, Hartmann A, Hajirezaei MR, von Wirén N. 2019. An age-dependent sequence of physiological processes defines developmental root senescence. *Plant Physiology* **181**(3): 993-1007.

Løes A-K, Gahoonia TS. 2004. Genetic variation in specific root length in Scandinavian wheat and barley accessions. *Euphytica* **137**(2): 243-249.

Lynch JP. 2013. Steep, cheap and deep: an ideotype to optimize water and N acquisition by maize root systems. *Annals of Botany* **112**(2): 347-357.

Lynch JP. 2015. Root phenes that reduce the metabolic costs of soil exploration: opportunities for 21st century agriculture. *Plant, Cell & Environment* **38**(9): 1775-1784.

Lynch JP. 2018. Rightsizing root phenotypes for drought resistance. *Journal of Experimental Botany* **69**(13): 3279-3292.

Maccaferri M, El-Feki W, Nazemi G, Salvi S, Canè MA, Colalongo MC, Stefanelli S, Tuberosa R. 2016. Prioritizing quantitative trait loci for root system architecture in tetraploid wheat. *Journal of Experimental Botany* **67**(4): 1161-1178.

Mancuso S, Boselli M. 2002. Characterisation of the oxygen fluxes in the division, elongation and mature zones of Vitis roots: influence of oxygen availability. *Planta* **214**(5): 767-774.

Maulana F, Ayalew H, Anderson JD, Kumssa TT, Huang W, Ma XF. 2018. Genome-Wide Association Mapping of Seedling Heat Tolerance in Winter Wheat. *Frontiers in Plant Science* **9**: 1272.

Maulana F, Kim K-S, Anderson JD, Sorrells ME, Butler TJ, Liu S, Baenziger PS, Byrne PF, Ma X-F. 2019. Genomic Selection of Forage Quality Traits in Winter Wheat. *Crop Science* **59**(6): 2473-2483.

McCormack ML, Guo D, Iversen CM, Chen W, Eissenstat DM, Fernandez CW, Li L, Ma C, Ma Z, Poorter H. 2017. Building a better foundation: Improving root‐trait measurements to understand and model plant and ecosystem processes. *New Phytologist* **215**(1): 27-37.

McCree K 1970. An equation for the rate of respiration of white clover grown under controlled conditions. *Prediction and measurement of photosynthetic productivity. Proceedings of the IBP/PP Technical Meeting, Trebon,[Czechoslovakia], 14-21 September, 1969*: Wageningen: PUDOC.

Meister R, Rajani M, Ruzicka D, Schachtman DP. 2014. Challenges of modifying root traits in crops for agriculture. *Trends in Plant Science* **19**(12): 779-788.

Messier J, Lechowicz MJ, McGill BJ, Violle C, Enquist BJ. 2017. Interspecific integration of trait dimensions at local scales: the plant phenotype as an integrated network. *Journal of Ecology* **105**(6): 1775-1790.

Mooney H. 1972. The carbon balance of plants. *Annual review of ecology and systematics* **3**(1): 315-346.

Müller B, Stich B, Piepho H. 2011. A general method for controlling the genome-wide type I error rate in linkage and association mapping experiments in plants. *Heredity* **106**(5): 825-831.

Ochoa IE, Blair MW, Lynch JP. 2006. QTL analysis of adventitious root formation in common bean under contrasting phosphorus availability. *Crop Science* **46**(4): 1609-1621.

Pagès L. 2014. Branching patterns of root systems: quantitative analysis of the diversity among dicotyledonous species. *Annals of Botany* **114**(3): 591-598.

Pan J, Li Z, Wang Q, Yang L, Yao F, Liu W. 2020. An S-domain receptor-like kinase, OsESG1, regulates early crown root development and drought resistance in rice. *Plant Science* **290**: 110318.

Parry G. 2014. Components of the Arabidopsis nuclear pore complex play multiple diverse roles in control of plant growth. *Journal of Experimental Botany* **65**(20): 6057-6067.

Poorter H, Lambers H, Evans JR. 2014. Trait correlation networks: a whole‐plant perspective on the recently criticized leaf economic spectrum. *New Phytologist* **201**(2): 378-382.

Poorter H, Van der Werf A, Atkin OK, Lambers H. 1991. Respiratory energy requirements of roots vary with the potential growth rate of a plant species. *Physiologia Plantarum* **83**(3): 469-475.

Porter HF, O'Reilly PF. 2017. Multivariate simulation framework reveals performance of multi-trait GWAS methods. *Scientific Reports* **7**: 38837.

R Core Team 2018. R: a language and environment for statistical computing. *Vienna, Austria: R Foundation for Statistical Computing.*

Rachmilevitch S, Cohen I, Huang B. 2015. Carbon allocation patterns into proteins and lipids associated with superior tolerance of perennial grass to high soil temperature. *Crop Science* **55**(5): 2262-2269.

Rajaram S 2001. Prospects and promise of wheat breeding in the 21 st century. *Wheat in a global environment*: Springer, 37-52.

Reich PB. 2014. The world‐wide 'fast‐slow' plant economics spectrum: a traits manifesto. *Journal of Ecology* **102**(2): 275-301.

Ren D, Fang X, Jiang P, Zhang G, Hu J, Wang X, Meng Q, Cui W, Lan S, Ma X. 2018. Genetic architecture of nitrogen-deficiency tolerance in wheat seedlings based on a nested association mapping (NAM) population. *Frontiers in Plant Science* **9**: 845.

Ripley B, Venables B, Bates DM, Hornik K, Gebhardt A, Firth D, Ripley MB. 2013. Package 'mass'. *Cran R* **538**.

Roell MS, Zurbriggen MD. 2020. The impact of synthetic biology for future agriculture and nutrition. *Curr Opin Biotechnol* **61**: 102-109.

Romero-Munar A, Del-Saz NF, Ribas-Carbó M, Flexas J, Baraza E, Florez-Sarasa I, Fernie AR, Gulías J. 2017. Arbuscular mycorrhizal symbiosis with Arundo donax decreases root respiration and increases both photosynthesis and plant biomass accumulation. *Plant, Cell & Environment* **40**(7): 1115-1126.

Roumet C, Birouste M, Picon-Cochard C, Ghestem M, Osman N, Vrignon-Brenas S, Cao K-f, Stokes A. 2016. Root structure-function relationships in 74 species: evidence of a root economics spectrum related to carbon economy. *New Phytologist* **210**(3): 815-826.

Sawada S-I. 1970. An ecophysiological analysis of the difference between the growth rates of young wheat seedlings grown in various seasons. *Journal of the Faculty of Science, University of Tokyo, 3 (Botany).* **10**(11/13): 233-263.

Scafaro AP, Negrini ACA, O'Leary B, Rashid FAA, Hayes L, Fan Y, Zhang Y, Chochois V, Badger MR, Millar AH, et al. 2017. The combination of gas-phase fluorophore technology and automation to enable high-throughput analysis of plant respiration. *Plant Methods* **13**: 16.

Schneider HM, Klein SP, Hanlon MT, Nord EA, Kaeppler S, Brown KM, Warry A, Bhosale R, Lynch JP. 2020. Genetic Control of Root Architectural Plasticity in Maize. *Journal of Experimental Botany* **71**(10): 3185–3197.

Schneider HM, Wojciechowski T, Postma JA, Brown KM, Lücke A, Zeisler V, Schreiber L, Lynch JP. 2017. Root cortical senescence decreases root respiration, nutrient content and radial water and nutrient transport in barley. *Plant, Cell & Environment* **40**(8): 1392-1408.

Seethepalli A, Guo H, Liu X, Griffiths M, Almtarfi H, Li Z, Liu S, Zare A, Fritschi FB, Blancaflor EB. 2020. Rhizovision crown: An integrated hardware and software platform for root crown phenotyping. *Plant Phenomics* **2020**: 3074916.

Seethepalli A, York LM 2020. RhizoVision Explorer - Software for image analysis of whole root systems and disconnected scanned roots. *Zenodo. DOI: 10.5281/zenodo.4095629*

Smith S, De Smet I 2012. Root system architecture: insights from Arabidopsis and cereal crops: The Royal Society.

Soriano JM, Alvaro F. 2019. Discovering consensus genomic regions in wheat for root-related traits by QTL meta-analysis. *Scientific Reports* **9**(1): 10537.

South PF, Cavanagh AP, Liu HW, Ort DR. 2019. Synthetic glycolate metabolism pathways stimulate crop growth and productivity in the field. *Science* **363**(6422).

Strock CF, De La Riva LM, Lynch JP. 2018. Reduction in root secondary growth as a strategy for phosphorus acquisition. *Plant Physiology* **176**(1): 691-703.

Sukumaran S, Reynolds MP, Sansaloni C. 2018. Genome-Wide Association Analyses Identify QTL Hotspots for Yield and Component Traits in Durum Wheat Grown under Yield Potential, Drought, and Heat Stress Environments. *Frontiers in Plant Science* **9**: 81.

Sun L, Ataka M, Han M, Han Y, Gan D, Xu T, Guo Y, Zhu B. 2020. Root exudation as a major competitive fine-root functional trait of 18 coexisting species in a subtropical forest. *New Phytologist*.

Thornley J. 1970. Respiration, growth and maintenance in plants. *Nature* **227**(5255): 304-305.

Turner SD. 2014. qqman: an R package for visualizing GWAS results using QQ and manhattan plots. *Biorxiv*: 005165.

Vriet C, Russinova E, Reuzeau C. 2012. Boosting crop yields with plant steroids. *The Plant Cell* **24**(3): 842-857.

Wang H, Hu Z, Huang K, Han Y, Zhao A, Han H, Song L, Fan C, Li R, Xin M. 2018. Three genomes differentially contribute to the seedling lateral root number in allohexaploid wheat: evidence from phenotype evolution and gene expression. *The Plant Journal* **95**(6): 976-987.

Wang S, Wong D, Forrest K, Allen A, Chao S, Huang BE, Maccaferri M, Salvi S, Milner SG, Cattivelli L, et al. 2014. Characterization of polyploid wheat genomic diversity using a

high-density 90,000 single nucleotide polymorphism array. *Plant Biotechnol J* **12**(6): 787-796.

Weber AP, Bar-Even A. 2019. Update: improving the efficiency of photosynthetic carbon reactions. *Plant Physiology* **179**(3): 803-812.

Xie Q, Fernando KM, Mayes S, Sparkes DL. 2017. Identifying seedling root architectural traits associated with yield and yield components in wheat. *Annals of Botany* **119**(7): 1115-1129.

Xu L, Zhao H, Ruan W, Deng M, Wang F, Peng J, Luo J, Chen Z, Yi K. 2017. ABNORMAL INFLORESCENCE MERISTEM1 functions in salicylic acid biosynthesis to maintain proper reactive oxygen species levels for root meristem activity in rice. *The Plant Cell* **29**(3): 560-574.

York LM. 2019. Functional phenomics: an emerging field integrating high-throughput phenotyping, physiology, and bioinformatics. *Journal of Experimental Botany* **70**(2): 379-386.

York LM, Nord E, Lynch J. 2013. Integration of root phenes for soil resource acquisition. *Frontiers in Plant Science* **4**: 355.

Yu P, Gutjahr C, Li C, Hochholdinger F. 2016. Genetic control of lateral root formation in cereals. *Trends in Plant Science* **21**(11): 951-961.

Zhou X, Stephens M. 2012. Genome-wide efficient mixed-model analysis for association studies. *Nature genetics* **44**(7): 821-824.

Zhou X, Stephens M. 2014. Efficient multivariate linear mixed model algorithms for genome-wide association studies. *Nature methods* **11**(4): 407.

Figure legends

Figure 1 Platform for phenotyping root respiration and other root traits of wheat seedlings. (a) Wheat seeds were surface sterilized and pre-germinated in plate, (b) Seedlings were grown in aerated hydroponics for 10 days, (c) Shoot and roots of seedling 10 days after transplanting, (d) Root respiration was measured in an airtight chamber using a LI-850 with temperature control using a bead bath, (e) Distinguished axial roots (blue) from lateral roots (red) of scanned image using RhizoVision Explorer. IRGA: Infrared gas analyzer, RC: Root chamber, BB: Bead bath, BF: Balston Filter.

Figure 2 (a) The relationship between predicted total root respiration and total root respiration, and deviations from the relationship results in new trait SRR_R, (b) Regression between specific root respiration by length and shoot dry weight.

Figure 3 Pairwise Pearson correlation of selected traits of TCAP winter wheat seedlings. The number represents the correlation values. Value marked with symbol × means correlation is not significant at p =0.05. Bright red to bright blue indicates highly positive to highly negative correlations. Trait abbreviations are as in Table 1.

Figure 4 (a) Scree graph showing percentage of variance explained by each of the first ten principal components, PCA variable contribution plots showing the (b) first and second PCs and (c) third and fourth PCs, where relative weightings of the variables are indicated by vectors. Trait abbreviations are as in Table 1.

Figure 5 Trait correlation network constructed from the Gaussian graphical model. Red and green edges show negative and positive correlations, respectively. The cutoff was set at 0.15.

Figure 6 Venn diagram of (a) associated SNPs cutoff set at $-\log_{10}P=3.5$, (b) genes identified using cutoff set at $-\log_{10}P= 3.5$ comparing significantly univariate of mean 25 traits, univariate analyses of 10 principal components (PCs), and multivariate of 6 trait combinations.

Figure 7 Manhattan plot of GWAS conducted on traits (a) SRR by mass, SRR by length, residuals of total respiration vs. volume of different segments, and multi-trait combination for root respiration, (b) SRL, AvgD, RTD, and multi-trait combination for root construction, (c) BP, BF, BD, and multi-trait combination for root topology of TCAP wheat population. Each dot represents a SNP. The horizontal black line indicates the threshold of significance at $-\log_{10}P = 3.5$.

Supporting Information

Figure S1 Histograms for the frequency distribution of 26 traits and 10 PC scores

Figure S2 Manhattan plots of GWAS conducted on all traits

Figure S3 Quantile-quantile (Q-Q) plots for all traits

Table S1 Centrality measures of 17 traits from Gaussian graphical model

Table S2 List of SNPs using a cutoff value set at $-\log_{10}P=3.5$

Table S3 List of nearest genes underlying SNPs using a cutoff value set at $-\log_{10}P=3.5$